Cable-Driven Jamming of a Boundary Constrained Soft Robot

Koki Tanaka,[1] Mohammad Amin Karimi,[1] Bruno-Pier Busque,[2] Declan Mulroy,[1] Qiyuan Zhou,[1]
Richa Batra,[3] Ankit Srivastava,[1] Heinrich M. Jaeger,[3] and Matthew Spenko[1]

***Abstract*— Soft robots employ flexible and compliant materials to perform adaptive tasks and navigate uncertain environments. However, soft robots are often unable to achieve forces and precision on the order of rigid-bodied robots. In this paper, we propose a new class of mobile soft robots that can reversibly transition between compliant and stiff states without reconfiguration. The robot can passively conform or actively control its shape, stiffen in its current configuration to function as a rigid-bodied robot, then return to its flexible form. The robotic structure consists of passive granular material surrounded by an active membrane. The membrane is composed of interconnected robotic sub-units that can control the packing density of the granular material and exploit jamming behaviors by varying the length of the interconnecting cables. Each robotic sub-unit uses a differential drive system to achieve locomotion and self-reconfigurability. We present the robot design and perform a set of locomotion and object manipulation experiments to characterize the robot's performance in soft and rigid states. We also introduce a simulation framework in which we model the jamming soft robot design and study the scalability of this class of robots. The proposed concept demonstrates the properties of both soft and rigid robots, and has the potential to bridge the gap between the two.**

I. Introduction

Soft robots are composed of compliant components and actuators [1], [2] that enable highly resilient behaviors such as manipulating objects of varying shapes or reconfigurability [3]–[5]. In contrast to most conventional robots, which consist of rigid links, soft robots have unique potential in applications including navigating unpredictable environments or interacting with humans in workplace settings [6], [7].

Despite the advantages afforded by soft robots, there remain significant challenges in modeling, controlling, and fabricating soft materials [8]–[10]. For example, soft robots that rely on thermal or electrical actuation are typically slow to respond and unable to apply large forces when compared to traditional robots [11], [12]. Pneumatically actuated soft robots, while more responsive and capable of applying larger forces, generally need to be tethered to external control mechanisms, which may preclude them from tasks that require lightweight, autonomous functionality [13], [14].

*This work was supported by NSF Grant #1830939. (*K. Tanka and M. A. Karimi are co-first authors. Corresponding author is K. Tanaka.*)

[1]K. Tanaka, M. A. Karimi, D. Mulroy, Q. Zhou, A. Sirvastava, and M. Spenko are with the Mechanical, Materials and Aerospace Department, Illinois Institute of Technology, Chicago, IL 60616, USA. ktanaka2@hawk.iit.edu, mkarimi1@hawk.iit.edu

[2]B. P. Busque is with the Department of Mechanical Engineering, Université de Sherbrooke, QC J1K 2R1, Canada.

[3]R. Batra and H. M. Jaeger are with the James Franck Institute, The University of Chicago, Chicago, IL 60637, USA.

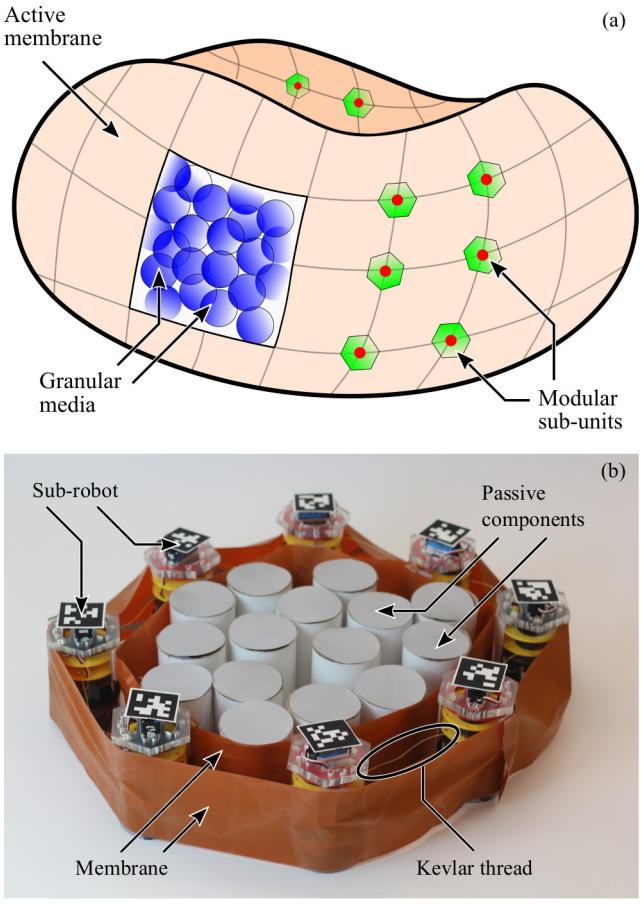

Fig. 1. (a) An illustration of the proposed jamming soft robot in three dimensions. The membrane comprises equally-spaced robotic sub-units, a selection of which are shown in green. A cut-out of the membrane reveals the interior granular material colored blue. (b) A two-dimensional prototype of the jamming soft robot concept.

Here we describe a mobile robot that can adaptively conform around objects and configure into various shapes while also controlling its rigidity. Rigidity is varied by exploiting jamming, where granular materials transition from a liquid-like to solid state through increasing pressure, density, shear stress or similar [15]. The robot consists of a passive granular material enclosed within a flexible membrane of robotic sub-units, which are capable of inducing jamming (see Fig. 1). While the membrane sub-units are unjammed, the robot maintains a soft body. Once the sub-units jam, the robot solidifies without significant reconfiguration. The robot is able to maintain its relative shape while stiffening, which is often difficult to achieve with soft materials [16], [17]. The

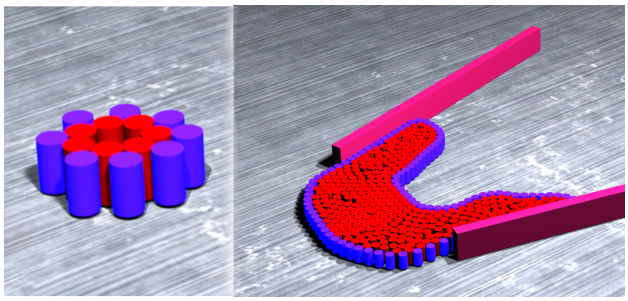

Fig. 2. Left: Simulation of a robot consisting of eight sub-units (indigo) and seven interior particles (red). Right: A robot with 100 active sub-units moving in a narrowing corridor.

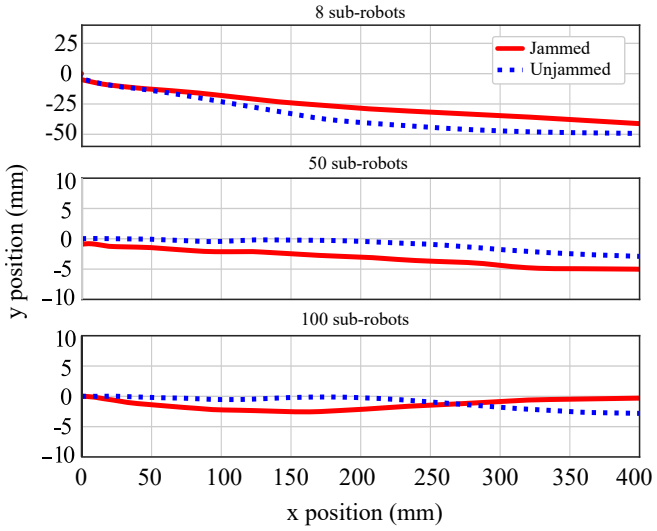

Fig. 3. The simulated robot's mean path in jammed and unjammed states.

paper describes a simulation framework that demonstrates the concept's scalability, the robot's mechanical design, and experimental validation of the approach.

Jamming has been utilized for robotic locomotion and manipulation before [18]. The universal gripper, for example, consisted of a latex membrane filled with granular material that can conform to an object in its unjammed state. Under a vacuum, the gripper stiffens around the object, allowing manipulation regardless of object morphology or fragility [19], [20]. Similarly, the Jamming Skin Enabled Locomotion robot is a spherical skin containing independently pressure-controlled pockets of granular media. By sequentially jamming and unjamming the pockets, the robot is able to roll and morph, demonstrating directed locomotion [21].

In the design presented here, we achieve jamming by reducing the robot's interior volume through cable-driven mechanisms that shorten the distance between neighboring sub-units, which locomote via differential drives. As shown in Fig. 1 (b), sub-units surround the white cylinders, serving as passive granular material. The latex membranes prevent any granules or objects from obstructing the cable mechanisms.

This paper is organized as follows: Section II presents the simulation framework and results, Section III details the design and controls of the robot prototype, Section IV describes the experimental setup and procedures, Section V explains the experimental results, and Section VI includes a summary and discussion of the work.

II. Modeling

A simulation of the prototype (see Fig. 2, left) allows us to investigate the system behavior more broadly and at larger scales (as shown in Fig. 2, right). The model is implemented using Project Chrono [22], a multibody dynamics library that uses non-smooth contact dynamics [23]. This dynamic method incorporates contact and collision forces as well as frictional effects.

A. Setup

Boundary sub-robots (120 g) and interior particles (40 g) are represented by ⌀80 mm, 120 mm tall cylinders. The interconnecting cables between boundary robots are modeled as virtual springs. Given that the cables only experience tension, the spring force parameters vary at every time step such that the springs are never in compression. Since there is no collision object associated with the virtual springs, the maximum distance between each sub-unit is defined so that interior granules cannot escape. The proximity of neighboring sub-units results in collisions between the interior granules and the sub-units, preventing the granules from moving between sub-units and outside the membrane boundary.

To validate the simulation, we calculate the packing fraction at which the jamming occurs. The packing fraction is determined by creating a Voronoi diagram, which defines the center position of each body as a node and forms a polygonal cell about the node based on the shortest distance to its neighbors. The areas of each cell is divided by the area of each body to determine the packing density. We vary design parameters, specifically membrane size and elasticity, in the model and calculate the jammed packing fraction. The membrane size was defined with respect to number of boundary sub-units, n_b, set between 10 and 80 units at increments of 10, and the string elasticity, defined by the virtual spring force, varied between 0.0 N and 3.0 N in 0.5 N increments. The packing fraction was not found to have any correlation to the boundary size or cable stiffness. Furthermore, the average packing fraction was found to be ϕ=.80 ($\pm$.03), which agrees with the literature on two dimensional granular systems [24].

Using the simulation framework, we study the robot locomotion with 8, 50, and 100 boundary units in both jammed and unjammed states (7, 90, and 345 internal particles, respectively). We also characterize the robot's ability to navigate through a narrow passage in which the gap is varied with respect to the robot size. In the simulations, the sub-robots locomote via open loop control with an initial velocity based on the initial boundary nodes' positions.

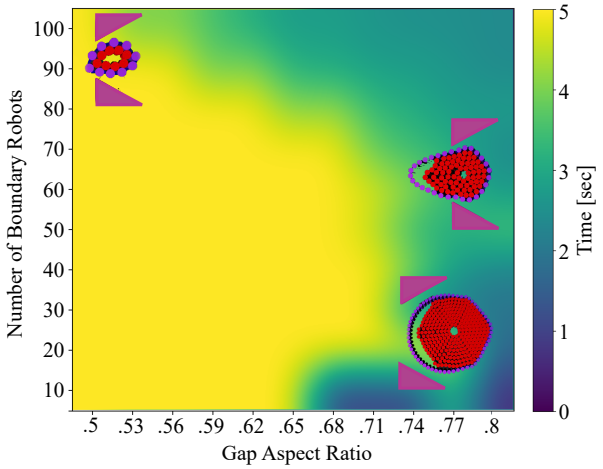

Fig. 4. Time taken to traverse a gap as a function of robot size and aspect ratio of gap to robot size. Times greater than 5 s indicate failure of the robot in the gap traversing take. Screenshots of the robot and gap configuration are shown for selected regions, with active robots in indigo, passive interior particles in red, and walls in pink.

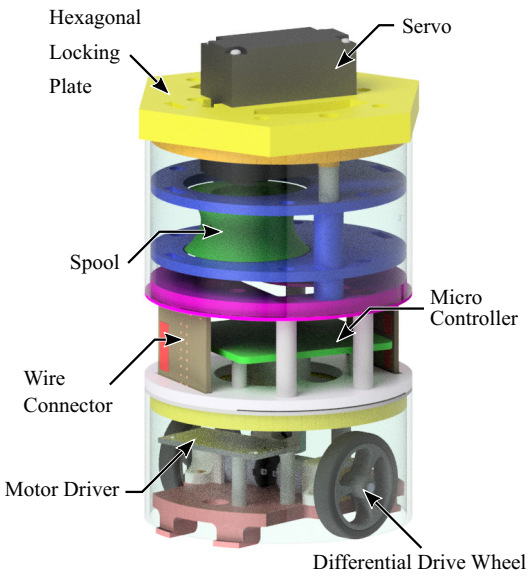

Fig. 5. CAD design of a sub-robot.

B. Simulation Results

Fig. 3 shows the path of the robot's geometric center for each scenario. As the number of sub-robots on the periphery increases, the robot better approximates a continuous system, and the noise that causes the robot with eight boundary sub-robots to deviate from its path is reduced, resulting in a lower locomotion error. The large-scale robot can also take advantage of its relative flexibility and ability for its passive interior to undergo granular shear flow, as is demonstrated in Fig. 2, which illustrates the robot's ability to change its shape while travelling through a narrowing corridor.

To better quantify the robot's increased conformability as a function of its size, another study investigates the effect of the number of sub-robots on the ability to traverse a narrow corridor of varying aspect ratios in relation to the robot (see Fig. 4). The coefficient of friction was kept at 0.4, as determined experimentally, while the driving force was scaled according to the mass of the entire system so that effects from increased friction with the ground are negated. Each boundary robots simply drives itself toward the narrowing corridor with a constant force.

The time required to traverse a gap of constant aspect ratio with respect to the robot can be used as a benchmark of the robot's conformability. Fig. 4 shows that the robot's performance is strongly related to the system size. For configurations with less than 70 boundary robots, the maximum traverseable gap decreases linearly, up to about 53% for a system of 100 boundary robots. This confirms the findings from the first study, which found that a system with a higher number of particles takes better advantage of its interior's ability to undergo granular shear flow and morph its shape to its environment.

III. Design of the Modular Robots

This section describes the mechanical and electrical design of the modular sub-unit robots.

A. Cable-Driven Jamming Mechanism

The robotic membrane consists of eight robotic sub-units (see Fig. 5). Each sub-unit is connected to its neighbors by 150 mm Kevlar thread (McMaster-Carr, 8800K44) spooled using a continuous rotation servo motor (SpringRC, SM-S4303R, 0.32 N m torque); each sub-unit actuates one cable connection. Hexagonal locking plates on the top of each sub-robot prevent rotation of the cylindrical sub-units during jamming. Without the flat surface and increased friction at the interface of the hexagonal plates, the membrane tends to form a circle during jamming instead of maintaining its current shape. The interior particles are ⌀80 mm 120 mm tall round tubes (McMaster-Carr 20545T28).

B. Mobility System

A differential drive system (Pololu, 298:1 Micro Metal Gearmotor MP 6 V) is located in the lower part, which can rotate independently from the top. This allows the heading angle for each sub-robot to be changed even when the top portion of the sub-robot is fully engaged in the jammed mode. A multi-turn rotational potentiometer (Bourns, 3856 - 3/4") tracks the relative rotation between the two parts.

C. Electrical Design

A Sparkfun SAMD21 micro-controller enables each sub-robot's control and communication. I^2C protocol is used for serial communication with a single sub-unit equipped with WiFi (Particle PHOTONH) to communicate with the user interface. The differential drive system uses a serial motor driver (Sparkfun ROB-13911). Power comes from an on-board 5 V/1 A LiPo battery (Sparkfun PRT-14411).

IV. Experimental Setup and Procedures

The experimental setup consists of a visual tracking system and a host computer running Robot Operating System (ROS) as described below.

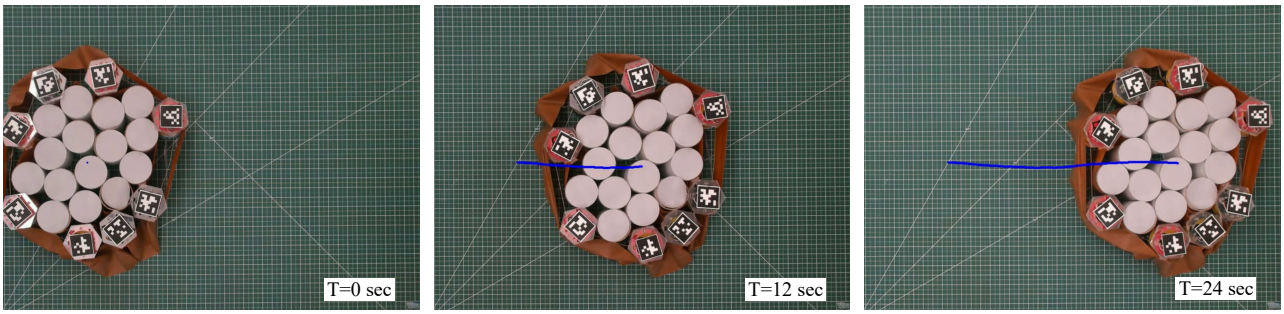

(a) Forward motion in jammed state with 15 interior particles

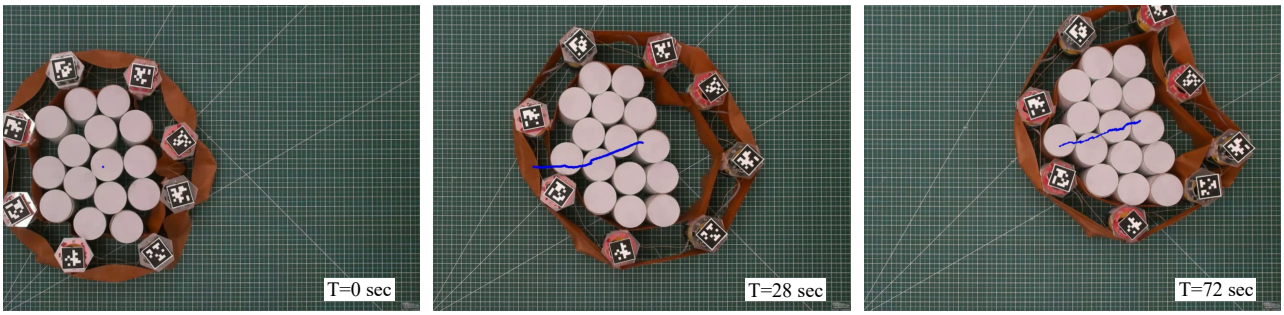

(b) Forward motion in unjammed state with 15 interior particles

Fig. 6. Locomotion of the robot in (a) jammed and (b) unjammed state. The trajectory of the geometric center of sub-robots is shown with a blue line.

A. Tracking System

The positions and orientations of sub-robots were tracked with a camera (Logitech, BRIO Ultra HD Pro Webcam) mounted above the experimental area. We used AprilTags on top of each sub-unit, which is a 2D barcode style tag that enables identifying the position and orientation of the sub-unit using visual feature detection [25].

B. Closed Loop Control System

Communication among the tracking system, controller, and sub-robots is accomplished through ROS. Each sub-unit's micro-controller reads the relative orientation of its top and bottom part and sends that data to the Photon micro-controller, which publishes it to the ROS interface. The tracking tags' poses are read by the camera and also published to ROS. The desired input values for all sub-robots is broadcast to the Photon micro-controller based on the heading angle of each sub-unit. Finally, the sub-robots receive the input values through I^2C communication with the micro-controller and execute the control command.

C. Experimental Procedures

The effect of the jamming phase transition was investigated by performing locomotion and grasping tasks in both jammed and unjammed states.

For the locomotion experiment, the heading angles of all sub-robots were initialized to 0°. Closed loop control was executed until the robot traveled at least 400 mm in the lateral direction. The experiment was conducted with both seven and fifteen inner, passive particles.

For the object handling test, two PVC cylindrical pipes (⌀57 mm, 62 mm height, 20 g and ⌀89 mm, 59 mm height, and 130 g) were grasped. The pipes were connected to a force gauge (Vernier, Dual-Range Force Sensor) by a string to measure the robot's pulling force. The robot and object's initial configuration were set manually before grasping the object. Six passive inner particles were used, and object manipulation was achieved by selectively activating only a portion of the sub-robots' jamming mechanisms. The latter is required because if all sub-robots were activated, the final configuration of the robot would be approximately circular, and the engulfed object would be expelled. After grasping the object, the robot pulled the object in a straight line.

V. Experimental Results and Discussion

A. Locomotion in Jammed and Unjammed States

Fig. 6 shows the robot's locomotion in both jammed and unjammed states. To ensure a jamming phase transition has occurred, the packing fraction ϕ is calculated based on the method described in Section II. The passive particles' position is estimated from the recorded video image by visual processing. For the jammed state, $\phi = 0.79$ and for the unjammed state, $\phi = 0.67$, which confirms that the jammed state is maintained during locomotion.

In the jammed state, the sub-robots and the passive particles are locked against each other and the entire robot moves as a rigid structure. In the unjammed state, the inner particles move freely inside the membrane. This changes the robot's center of mass during locomotion. Therefore, despite using the same closed loop control, the robot's heading angle deviates more during unjammed locomotion.

The reaction force from the passive components also accounts for locomotion errors. As the robot moves to

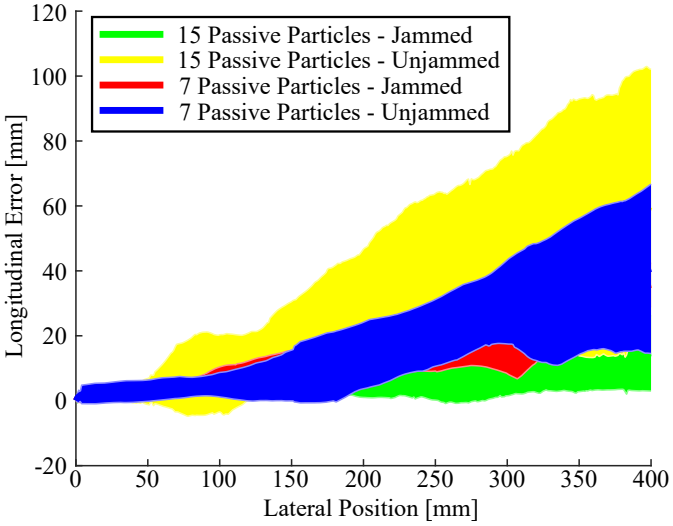

Fig. 7. Longitudinal error over the trajectory for jammed and unjammed state with seven and 15 particles.

the right, the inner particles shift to the left (see Fig. 6 (b) at T = 28 s and T = 72 s). Consequently, the load distribution among the sub-robots is not uniform and the sub-robots move different distances. In the jammed state, all of the sub-robots contribute to the transport of the inner particles approximately equally. Thus, the jamming phase transition can be utilized to achieve a more accurate and robust locomotion when conformability is not needed. The conformability can be easily restored when it is necessary, for example to traverse the narrow corridor as showed in Fig. 2. We expect that unjammed locomotion is preferred when obstructions are present in the environment, given its ability to adapt and yield in the unjammed state.

The absolute error in the longitudinal direction over the trajectory is shown in Fig. 7 for four trials each. For both seven and 15 passive particles, the jammed state showed a lower error and standard deviation than the unjammed state. The more particles, the less trajectory error was observed especially for the jammed state. This result shows the potential of scalability of the proposed robot for robust locomotion.

The average longitudinal error for the seven passive particles case is compared with the simulation results. The experimental and simulation results show an average 27% and 29% improvement with the jammed state, respectively. This comparison also shows a reasonable qualitative match between the simulation and experimental results.

Fig. 8 shows the elapsed time to travel 400 mm in the lateral direction. For both the fewer and greater numbers of passive components, the jammed robot moved faster than the unjammed one. Note that in the test with fifteen passive particles, the desired speed input of the subrobots was increased by 20% to facilitate locomotion.

B. Grasping and Pulling an Object

Fig. 9 shows the robot grasping two objects of different sizes by performing a jamming operation. The aspect ratio

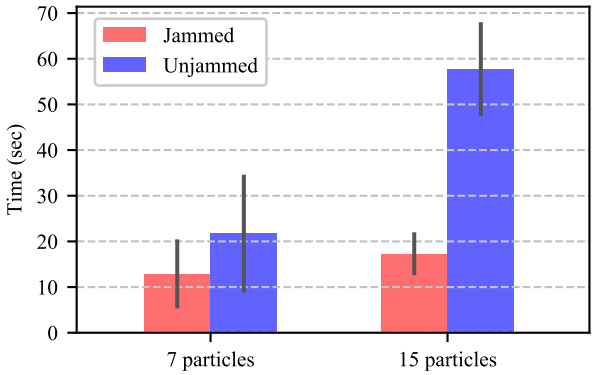

Fig. 8. Travel time for 400 mm lateral locomotion. Error bars show the standard deviation.

(a) Small object (concealed by the membrane)

(b) Large object

Fig. 9. Grasping small (a) and large (b) objects by selective jamming. The object is indicated by a blue circle and the sub-robots activated for jamming are marked by the red line.

of grasped objects to robot overall size is 0.14 for the small object and 0.22 for the large object. The sub-robots that were performed the jamming are highlighted in red. Note that the smaller object was grasped by the interlocking behaviour of the sub-robots. The larger object, on the other hand, was only pinched by two neighboring sub-robots. The grasping configuration is mostly determined by the scale of the object compared to the robot, and the infill density and size of the passive particles. While the robot engulfs the grasped object, it maintains the unjammed state to deform its shape and to confirm to the object. We expect the quality of the grasp to improve with larger numbers of sub-robots and passive particles.

Fig. 10 shows the maximum pulling force that was exerted on the grasped object in the jammed and unjammed states. The jammed case outperformed the unjammed one for both object sizes. The robot can exert a pulling force on the small object even in the unjammed state, while for the large object the pulling force was effectively zero in unjammed state. This can be attributed to the interlocking behaviour of the sub-units for small objects, whereas the large object is grabbed mainly by friction between the object and the membrane.

VI. Conclusions

This paper presents a mobile robot capable of transitioning between rigid and soft modes by exploiting the jamming phase transition of granular materials. In the robot, a granular media is confined by a flexible membrane with rigid sub-robots that employ length-varying cables to manipulate

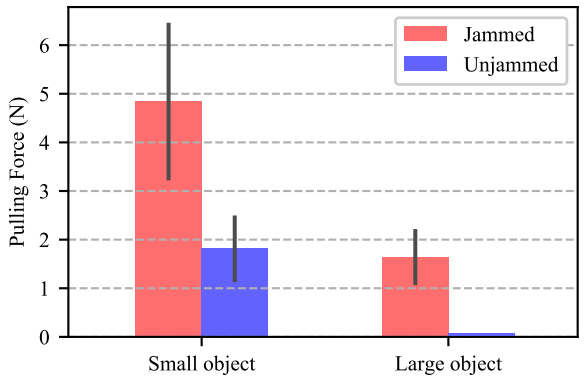

Fig. 10. Pulling force exerted to the grasped object. Error bars show the standard deviation. Note that in the unjammed state, the pulling force is zero for the large object.

the packing density of the internal volume. A simulation framework demonstrated the robot's performance at greater scales and in challenging environments, demonstrating the potential of this concept for different applications. We also developed a prototype to study the effects of jamming with respect to locomotion and grasping force. Results showed that locomotion is more efficient and larger forces are exerted on the objects when the robot is rigid.

There are several differences between the simulation and the experimental prototypes. For example, the simulated boundary robots are linked with springs that are able to dynamically change stiffness while the experimental sub-robots are linked via cables and a flexible fabric. Additionally, the prototype's differential drives are represented by a single external force applied to each robot in the simulation. Nonetheless, both the simulation and prototype demonstrated a mobile robot that can transition between soft and rigid states. The simulations provide a high level perspective of the concept and are meant to investigate the theoretical behavior of a larger system. The prototype demonstrates the robot's feasibility and potential. We plan to further utilize this work as we explore potential control strategies and designs.

Acknowledgments

The authors thank Kristen Such for her assistance on the PCB design, Alister Mcgrath and Michael Ogiela for their assistance in the sub-robot fabrication, and Michael Bonthron for post-processing the recorded experimental videos.

References

[1] D. Rus and M. T. Tolley, "Design, fabrication and control of soft robots," *Nature*, vol. 521, no. 7553, p. 467, 2015.

[2] S. Kim, C. Laschi, and B. Trimmer, "Soft robotics: a bioinspired evolution in robotics," *Trends in biotechnology*, vol. 31, no. 5, pp. 287–294, 2013.

[3] J. W. Booth, D. Shah, J. C. Case, E. L. White, M. C. Yuen, O. Cyr-Choiniere, and R. Kramer-Bottiglio, "OmniSkins: Robotic skins that turn inanimate objects into multifunctional robots," *Science Robotics*, vol. 3, no. 22, sep 2018.

[4] J. Hughes, U. Culha, F. Giardina, F. Guenther, A. Rosendo, and F. Iida, "Soft Manipulators and Grippers: A Review," *Frontiers in Robotics and AI*, vol. 3, no. NOV, pp. 1–12, nov 2016.

[5] S. Miyashita, S. Guitron, S. Li, and D. Rus, "Robotic metamorphosis by origami exoskeletons," *Science Robotics*, vol. 2, no. 10, sep 2017.

[6] M. Cianchetti, T. Ranzani, G. Gerboni, T. Nanayakkara, K. Althoefer, P. Dasgupta, and A. Menciassi, "Soft robotics technologies to address shortcomings in today's minimally invasive surgery: the stiff-flop approach," *Soft robotics*, vol. 1, no. 2, pp. 122–131, 2014.

[7] F. Iida and C. Laschi, "Soft Robotics: Challenges and Perspectives," *Procedia Computer Science*, vol. 7, pp. 99–102, 2011.

[8] E. Coevoet, T. Morales-Bieze, F. Largilliere, Z. Zhang, M. Thieffry, M. Sanz-Lopez, B. Carrez, D. Marchal, O. Goury, J. Dequidt, and C. Duriez, "Software toolkit for modeling, simulation, and control of soft robots," *Advanced Robotics*, vol. 31, no. 22, pp. 1208–1224, 2017.

[9] T. George Thuruthel, Y. Ansari, E. Falotico, and C. Laschi, "Control Strategies for Soft Robotic Manipulators: A Survey," *Soft Robotics*, vol. 5, no. 2, pp. 149–163, 2018.

[10] H. Lipson, "Challenges and opportunities for design, simulation, and fabrication of soft robots," *Soft Rob.*, vol. 1, no. 1, pp. 21–27, 2014.

[11] K. Zhang, C. Qiu, and J. S. Dai, "Helical Kirigami-Enabled Centimeter-Scale Worm Robot With Shape-Memory-Alloy Linear Actuators," *J. Mechanisms and Robotics*, vol. 7, no. 2, 2015.

[12] C. Laschi, M. Cianchetti, B. Mazzolai, L. Margheri, M. Follador, and P. Dario, "Soft robot arm inspired by the octopus," *Advanced Robotics*, vol. 26, no. 7, pp. 709–727, 2012.

[13] E. W. Hawkes, L. H. Blumenschein, J. D. Greer, and A. M. Okamura, "A soft robot that navigates its environment through growth," *Science Robotics*, vol. 2, no. 8, jul 2017.

[14] R. F. Shepherd, F. Ilievski, W. Choi, S. A. Morin, A. A. Stokes, A. D. Mazzeo, X. Chen, M. Wang, and G. M. Whitesides, "Multigait soft robot," *P. Nat. Acad. Sciences*, vol. 108, no. 51, pp. 20 400–20 403, 2011.

[15] M. van Hecke, "Jamming of soft particles: geometry, mechanics, scaling and isostaticity," *J. Physics: Condensed Matter*, vol. 22, no. 3, 2009.

[16] T. P. Chenal, J. C. Case, J. Paik, and R. K. Kramer, "Variable stiffness fabrics with embedded shape memory materials for wearable applications," in *IEEE IROS*. Institute of Electrical and Electronics Engineers Inc., oct 2014, pp. 2827–2831.

[17] Y. Hao, T. Wang, X. Fang, K. Yang, L. Mao, J. Guan, and L. Wen, "A variable stiffness soft robotic gripper with low-melting-point alloy," in *Chinese Control Conference, CCC*. IEEE Computer Society, sep 2017, pp. 6781–6786.

[18] E. Steltz, A. Mozeika, J. Rembisz, N. Corson, and H. M. Jaeger, "Jamming as an enabling technology for soft robotics," in *Electroactive Polymer Actuators and Devices (EAPAD) 2010*, Y. Bar-Cohen, Ed., vol. 7642, no. April 2010, mar 2010.

[19] E. Brown, N. Rodenberg, J. Amend, A. Mozeika, E. Steltz, M. R. Zakin, H. Lipson, and H. M. Jaeger, "Universal robotic gripper based on the jamming of granular material," *Proceedings of the National Academy of Sciences*, vol. 107, no. 44, pp. 18 809–18 814, 2010.

[20] J. R. Amend, E. Brown, N. Rodenberg, H. M. Jaeger, and H. Lipson, "A positive pressure universal gripper based on the jamming of granular material," *IEEE Transactions on Robotics*, vol. 28, no. 2, pp. 341–350, 2012.

[21] E. Steltz, A. Mozeika, J. Rembisz, N. Corson, and H. Jaeger, "Jamming as an enabling technology for soft robotics," in *Electroactive Polymer Actuators and Devices (EAPAD) 2010*, vol. 7642. International Society for Optics and Photonics, 2010.

[22] A. Tasora, R. Serban, H. Mazhar, A. Pazouki, D. Melanz, J. Fleischmann, M. Taylor, H. Sugiyama, and D. Negrut, "Chrono: An open source multi-physics dynamics engine," *High Performance Computing in Sci. and Eng.–Lec. Notes in Comp. Sci.*, pp. 19–49, 2016.

[23] F. Pfeiffer and C. Glocker, *Multibody Dynamics with Unilateral Contacts*. Springer-Verlag Wien, 1996.

[24] S. Nezamabadi, T. H. Nguyen, J.-Y. Delenne, and F. Radjai, "Modeling soft granular materials," *Granular Matter*, vol. 19, no. 1, p. 8, feb 2017. [Online]. Available: http://link.springer.com/10.1007/s10035-016-0689-y

[25] J. Wang and E. Olson, "AprilTag 2: Efficient and robust fiducial detection," in *2016 IEEE/RSJ International Conference on Intelligent Robots and Systems (IROS)*. IEEE, oct 2016, pp. 4193–4198.